Co-operative Programme for Monitoring and Evaluation of the Long Range Transmission of Air Pollutants in Europe

EMEP

MSC-E

Meteorological Synthesizing Center - EAST

REGIONAL MODELS LPMOD AND ASIMD. ALGORITHMS, PARAMETRIZATION AND RESULTS OF APPLICATION TO PB AND CD IN EUROPE SCALE FOR 1990

M.Pekar

EMEP / MSC-E Report 9/96

August 1996

Kedrova str. 8-1, Moscow, Russia
Tel. 007 095 124 47 58
Fax 007 095 310 70 93
E-Mail MSCE@ GLASNET.SU

Contents

Preface and acknowledgement

In accordance with the decision of the EMEP Executive Body (ECE/EB.AIR/42, December 14, 1994) modelling of Heavy Metals and Persistent Organic Pollutants is the subject of the sixth phase of the EMEP activities. In order to include HM and POPs into modelling within the framework of EMEP MSC-E undertook the modernization of the operational model and the development of the more sophisticated Eulerian models. This report presents two four-layer Eulerian models for HM. Those models took part in the intercomparison of modelling for HM made by MSC-E in 1995/96 according to the recommendation of the EMEP Steering Body.

The report presents model descriptions, statistics of meteoparameters adopted for the boundary layer, results of the model applications to Pb and Cd for 1990, some analysis including the comparison with available measurements and comparison between the models.

The author is grateful to Irina Nikiforova for supplying with multiple maps of the different grid patterns.

1 Introduction

Recent decades heavy metals emitted by anthropogenic sources have been of environmental problem concern. Heavy metals behave in the atmosphere mainly as aerosols. The shape of the atmospheric particle size distribution varies both spatially and temporally. The part of that variability can be attributed to the differences of primary particulate emissions, while the rest of it is the result of various aerosol phenomena taking place in the atmosphere. The measured mass size distributions were found to be the function of the volatility of the substance which can be related to the melting and boiling points [1].

Aerosols with Pb and Cd are associated with high temperature technologies and they are characterized by the mass median diameter (MMD) less then 1 μm [1]. Nearly identical relative size distributions were observed in polluted and remote areas [1, 2, 3]. In the most cases the mass size distributions for each of the elements were log-normal [2]. It is supposed that the steady-state equilibrium of the relative size distributions is shaped quickly - not far away from the sources [4].

Several models are available for describing the dry deposition velocity of particles as a function of particle size. Among them the model of *Sehmell and Hodgson* [5] and the model of Williams [6] for deposition to the water surface are widely practised. An appraisal of current knowledge of particle dry deposition was given by *Ruijgrok et al* [7]. Specifically *van Aalst`s* results of comparison of dry deposition velocities estimated by above-mentioned models are presented there. And an essential difference (about one order of magnitude) are noted for deposition velocities of 1 μm particles for the controlled roughness conditions. Since the model of Williams takes into account hygroscopic growth of particles and their capture by waves, calculated velocities are significantly higher.

The wet deposition, that is, absorption into droplets followed by droplet removal during precipitation is a competitive pathway. The wet scavenging efficiency depends on many processes. For aerosols they are mainly nucleation, Brownian diffusion and impaction. The wet deposition is the final result of the scavenging of particles by cloud droplets (rainout) and rainfall (washout) with differences of collection efficiency. The efficiency of subcloud scavenging is strongly dependent on particle and drop sizes [8] since it relates to the efficiency of their collision. The curve of the dependence of collision efficiency on particle sizes has its minimum for 0.1-1 μm particles differing 3-4 orders of magnitude from the collision efficiency of either coarse particles (~10 μm) or submicron particles ($\sim 10^{-3}$ μm). For the assessment of particle scavenging in a cloud Junge`s approach is used [9] where the local concentration of aerosol in cloud water is proportional to the air concentration and varies inversely from the liquid water contents of rain at any level. However, recent investigations indicate that Junge`s relation is violated at intense precipitation [10], the dilution effect is more important for aerosol scavenging than for gas scavenging. While modelling the long-term transport it is often impossible to simulate isolated clouds therefore empirical data on the relationship of concentrations in air and precipitations is used for the parametrization of the resulting scavenging process.

Finally while the modelling of Pb and Cd dispersion in Europe we are based on the following provisions. Heavy metals in the process of transport and deposition are considered as fine aerosols

characterized by some effective particle sizes. Though the data indicate that in mass spectrum there is a small part of heavy particles for which is necessary to take into account settling process however for the long-range transport the weightless component is the most important. While the simulation of the interaction with the surface we started from the models of Sehmel, 1980 [5] - for land and of Williams, 1982 [6] - for sea. Scavenging with precipitations is realized by a simple method based on empirical data on integral scavenging ratio without distinction between in-cloud and subcloud scavenging.

HM long-range modelling within the European region is carried out by a number of investigators [11-14] using for operational modelling relatively simple models more often of Lagrangian type. While in choosing Lagrangian models such principal disadvantage of Eulerian models as numerical viscosity is important and horizontal transport is of the decisive importance among processes considered by large-scale models.

At present there is a definite trend of the improvement of spatial resolution of models and correspondingly of the input information for them. Under those circumstances it is obviously necessary to take into account the vertical structure of the boundary layer (wind shear, vertical turbulent exchange, diurnal variations, interaction with the troposphere) as well as the emission vertical distribution. The problem can be resolved by three-dimensional Eulerian modelling since an application of trajectory models in the conditions of the wind shear and vertical exchange encounters great difficulties. As far as numerical viscosity of Eulerian models is concerned numerous studies aimed at the minimization of those inaccuracies resulted in the development of algorithms with the high accuracy though with extra computer resources.

The Eulerian model versions LPMOD and ASIMD are developed at MSC-E. The present purpose of the models are to provide calculations of the atmospheric depositions and concentrations of heavy metals within the European scale.

The basic model is Large Particle Model (LPMOD) in which numerical transport scheme with the conservation of 6 moments of the particle grid distribution within the cell is used [15]. The scheme makes it possible to regulate the model dissipativity properties by the introduction of subgrid diffusion. The model structure modified for sulphur compounds is described in [16]. The model version for heavy metals modelling is described in this report.

ASIMD model is called so because of the application to it of an asymmetric advection scheme also developed in MSC-E [17]. In particular that scheme was used in 3-dimensional model which participated in ATMES project [18]. That algorithm may be compared with Smolarkewiz scheme [19] their difference is in the fact that our non-linear anti-diffusion correction is derived analytically that makes it possible to obtain the solution at a step without iterations. At first it was supposed that ASIMD would be used as a supplementary model to LPMOD for comparison and evaluation of the dissipation effect. Taking into account that the LPMOD is “more expensive” at first the parametrization of the boundary layer and of scavenging processes were also evaluated by fasted ASIMD.

The input meteoinformation is quantized with 150 km resolution, ASIMD model has an appropriate resolution the same time LPMOD provides fields with 75-km resolution. A finer resolution for calculations within the European scale for the period of about one year seems to be premature since the required degree of verification of the accuracy and interconnection of a great number of parameters lacks.

Parallel calculations made with LPMOD and ASIMD show that their results are similar for the case of the long-term integration with multiple sources. ASIMD may be used as an original model. Further all results received with both models will be presented in comparative way.

2 General structure of LPMOD, ASIMD models

2.1 Formulation of the problem and space discretization

The dispersion process of passive pollution in the atmospheric boundary layer is described by equation:

$$\frac{\partial C}{\partial t} + u\frac{\partial C}{\partial x} + v\frac{\partial C}{\partial y} = K_H\left(\frac{\partial^2 C}{\partial x^2} + \frac{\partial^2 C}{\partial y^2}\right) + \frac{\partial}{\partial z}K_Z\frac{\partial C}{\partial z} - \Lambda C + Q, \qquad (1)$$

where t - time; x,y,z - Cartesian co-ordinates; $C(x,y,z,t)$ - concentration; $u(x,y,z,t)$, $v(x,y,z,t)$ - wind speed components; K_H=constant, $K_Z(x,y,z,t)$ - horizontal and vertical diffusion coefficients; Λ - coefficient of precipitation scavenging; $Q(x,y,z,t)$ - emission.

As the initial condition the background distribution may be assumed:

$$C\,(x,y,z,t = 0) = f(x,y,z) \qquad (2)$$

For the initialization of background concentration a long start-up period (5 days) is used.

At the lower boundary $z = z_0$ (z_0 - roughness length) a flux depending on pollution and surface types is assumed:

$$\left(-K_Z\frac{\partial C}{\partial z}\right)_{z=z_0} = F_0(x,y,t) \qquad (3)$$

At the upper boundary the positive diffusion flux is determined by local (small) diffusion coefficient (or equal to zero):

$$\left(-K_Z\frac{\partial C}{\partial z}\right)_{z=h} = F_h(x,y,t) \qquad (4)$$

The lateral boundaries are assumed to be free.

In this formulation the problem is solved by a numerical method using 3-dimensional grid with assumed resolution multiple to the EMEP square Δx=Δy=150 km. The calculations presented are made on grid 80×76×4 (Δx=Δy=75 km) with the LPMOD model and 39×37×4 (Δx=Δy=150 km) with the ASIMD model. The wind, temperature and precipitation fields are gridded with gridsize 150 km. Meteoelements were not interpolated in the LPMOD grid in these calculations. Practically LPMOD uses two half-steps for advection and vertical diffusion for one time step which is used for other processes.

Along the vertical a non-uniform grid with four layers is taken, fig.1. The surface layer, Δz =100 m is separated, the depths of the following layers are chosen with orientation to the levels of meteorological data. The calculated levels along z correspond to cell centers.

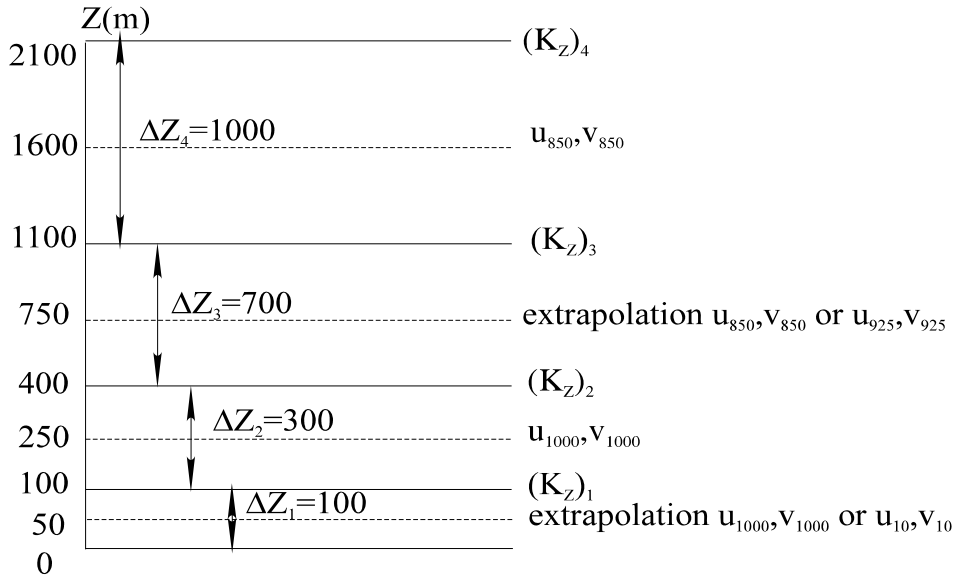

Fig.1: *Vertical grid of the model. Levels at which meteoparameters are specified: u_{850},v_{850} - winds of the level of 850 mb; u_{1000},v_{1000} - winds of the level of 1000 mb; u_{10},v_{10} - winds of the level of 10 m. $(K_z)_i$ - grid values of $K_z(z)$ profile.*

The solution is realized by integration relative to time with step τ = 1 h using the technique of operator (1) splitting:

- horizontal transport and diffusion;
- vertical diffusion;
- dry deposition;
- scavenging with precipitation.

The model operates with analysed meteorological data provided by Hydrometcentre of Russia. Before 1995 MSC-E had data on wind fields at levels 1000 mb, 850 mb, temperature at the level 1000 mb and precipitation events. The meteorological data are averaged over 6 hours.

The adaptation of the model to this data base was made in the following way:

The wind at 1000 mb corresponds to the second layer along the vertical (z = 250 m); the wind 850 mb corresponds to the fourth layer (z =1600 m); the wind for the third layer (z=750 m) is determined by extrapolation: u_3=0.8·u_{850}, v_3=0.8·v_{850}; the surface wind is obtained by extrapolation of 1000 mb wind to the level of 50 m after the evaluation of the boundary layer stability.

Since 1995 this database is appreciably extended in addition to the above mentioned information we have the wind at levels 925 mb, 700 mb, temperature at all levels, cloudiness. In this case wind at 925 mb is for the third layer (z = 750 m). Temperature and wind define stability of each layer and correspondingly profiles $K_z(z)$.

3 Numerical methods

3.1 Horizontal transport and diffusion in LPMOD

In accordance with the above mentioned splitting scheme the following equation is solved:

$$\frac{\partial C}{\partial t} + u\frac{\partial C}{\partial x} + v\frac{\partial C}{\partial y} = K_H\left(\frac{\partial^2 C}{\partial x^2} + \frac{\partial^2 C}{\partial y^2}\right). \qquad (1)$$

The algorithm is described in [15]. In brief it comprises the following. Pollution is imitated by an ensemble of mobile elements with size of double grid intervals (large particles) for which co-ordinates of mass centers are calculated. (We shall operate with masses and not concentrations, it is not principal since elements are standard $M = C \cdot 4\Delta x \Delta y \Delta z$). The transport of elements with local velocities corresponds to advection. At the same time 6 moments are stored for each cell. Next step begins with the reconstruction of distribution in a cell. It is represented with 4 elements which masses and co-ordinates are calculated keeping exact conservativity of all moments. Here physical diffusion which is of subgrid origin and may be small is introduced. The cycle is completed with advection of these elements and accumulation of moments for the next step.

The algorithm for one step is as follows (Sketch 1):

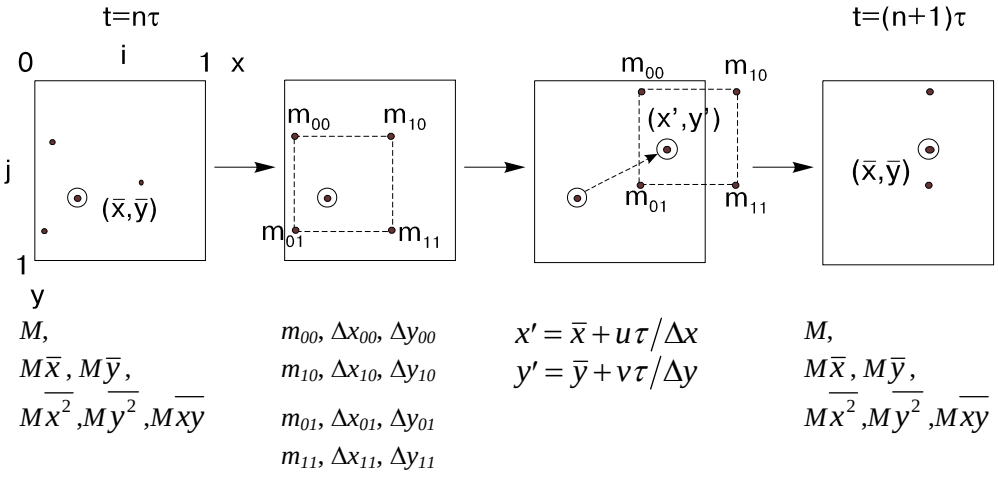

Sketch 1: *Advection scheme for one ij-cell at one time step. (for example three initial elements are taken). Symbols down boxes correspond to values calculated step by step (see text).*

- element mass centers, ⊙ - mass center of whole distribution

a) Initially for cell (i,j) we have 6 moments:

$$\mathrm{M},\ \mathrm{M}\bar{x},\ \mathrm{M}\bar{y},\ \mathrm{M}\overline{x^2},\ \mathrm{M}\overline{y^2},\ \mathrm{M}\overline{xy}; \tag{2}$$

distribution parameters (2) are determined:

$$\bar{x} = \mathrm{M}\,\bar{x}/\mathrm{M};\ \bar{y} = \mathrm{M}\,\bar{y}/\mathrm{M};\ \sigma_x^2 = \mathrm{M}\,\overline{x^2}\big/\mathrm{M} - \bar{x}^2;$$
$$\sigma_y^2 = \mathrm{M}\,\overline{y^2}\big/\mathrm{M} - \bar{y}^2;\ \ \mathrm{cov} = \mathrm{M}\,\overline{xy}/\mathrm{M} - \bar{x}\,\bar{y}, \tag{3}$$

(hereinafter bars will be omitted)

b) Then the reconstruction of distribution (2) to explicit 4-mass distribution is made.

Bearing in mind that x and y can be close to 0 or 1 the transformation:

$$x' = 0.25 + abs\,(abs\,(x - 0.75) - 0.5)$$
$$y' = 0.25 + abs\,(abs\,(y - 0.75) - 0.5) \tag{4}$$

allows to make the reconstruction in a suitable co-ordinate system - either in the initial system or in the system with the shift by half step to the right or to the left.

At “upwind” distribution with grid knots we have variances:

$$\sum_x^2 = x'(1 - x') \geq \sigma_x^2, \quad \sum_y^2 = y'(1 - y') \geq \sigma_y^2, \tag{5}$$

which are relevant scales for σ_x^2 and σ_y^2.

Then scale factors are calculated:

$$\alpha^2 = \frac{\sigma_x^2}{\bar{x}(1-\bar{x})}; \qquad \beta^2 = \frac{\sigma_y^2}{\bar{y}(1-\bar{y})}. \tag{6}$$

The covariance conservation is achieved by its transformation:

$$\begin{aligned} \mathrm{cov}^* &= \min\left[\bar{x}(1-\bar{y}), \bar{y}(1-\bar{x}), \frac{\mathrm{cov}}{\alpha\beta}\right], \qquad \text{if } \mathrm{cov}>0 \\ \mathrm{cov}^* &= -\min\left[(1-\bar{y})(1-\bar{x}), \bar{x}\bar{y}, \frac{\mathrm{cov}}{\alpha\beta}\right], \quad \text{if } \mathrm{cov}<0 \end{aligned} \tag{7}$$

c) Desired masses are determined:

$$\begin{aligned} m_{00} &= \mathrm{M}\left[(1-\bar{x})(1-\bar{y}) + \mathrm{cov}^*\right] \\ m_{10} &= \mathrm{M}\left[\bar{x}(1-\bar{y}) - \mathrm{cov}^*\right] \\ m_{01} &= \mathrm{M}\left[(1-\bar{x})\bar{y} - \mathrm{cov}^*\right] \\ m_{11} &= \mathrm{M}\left[\bar{x}\bar{y} + \mathrm{cov}^*\right] \end{aligned} \tag{8}$$

d) Their co-ordinates relative to $\bar{x},\bar{y}$ are equal:

$$\begin{aligned} \Delta x_{00} &= -\alpha\bar{x}, & \Delta y_{00} &= -\beta\bar{y}; \\ \Delta x_{10} &= \alpha(1-\bar{x}), & \Delta y_{10} &= -\beta\bar{y}; \\ \Delta x_{01} &= -\alpha\bar{x}, & \Delta y_{01} &= \beta(1-\bar{y}); \\ \Delta x_{11} &= \alpha(1-\bar{x}), & \Delta y_{11} &= \beta(1-\bar{y}); \end{aligned} \tag{9}$$

(indices are determined by the co-ordinate system in a given cell:

00 correspond to knot ($\bar{x}$ = 0, $\bar{y}$ = 0); 10 - ($\bar{x}$ =1, $\bar{y}$ = 0); 01 - ($\bar{x}$ =0, $\bar{y}$ = 1); 11 - ($\bar{x}$ =1, $\bar{y}$ = 1)).

e) Final step - advection of the en

semble as a whole:

$$x' = x + \frac{u\tau}{\Delta x}; \quad y' = y + \frac{v\tau}{\Delta y}; \tag{10}$$

(here x and y are true co-ordinates of mass center determinated by formulas (3)).

Relative co-ordinates of particles (9) (now relative to x',y') define their allocation to cells that makes it is possible to sum them up for the accumulation of moments (2) for next n+1 step.

Zero moments-masses are not desired values because they have different co-ordinates and variances. True distributions are obtained at the expansion of a family of elements attributed to each cell in cell knots. This expansion for elements of double size is (Sketch 2):

$$\begin{aligned} \Delta m_{00} &= \mathrm{M} - \mathrm{M}\,\bar{x} - \mathrm{M}\,\bar{y} + \mathrm{M}\,\overline{xy}; \\ \Delta m_{10} &= \mathrm{M}\,\bar{x} - \mathrm{M}\,\overline{xy}; \\ \Delta m_{01} &= \mathrm{M}\,\bar{y} - \mathrm{M}\,\overline{xy}; \\ \Delta m_{11} &= \mathrm{M}\,\overline{xy}, \end{aligned} \tag{11}$$

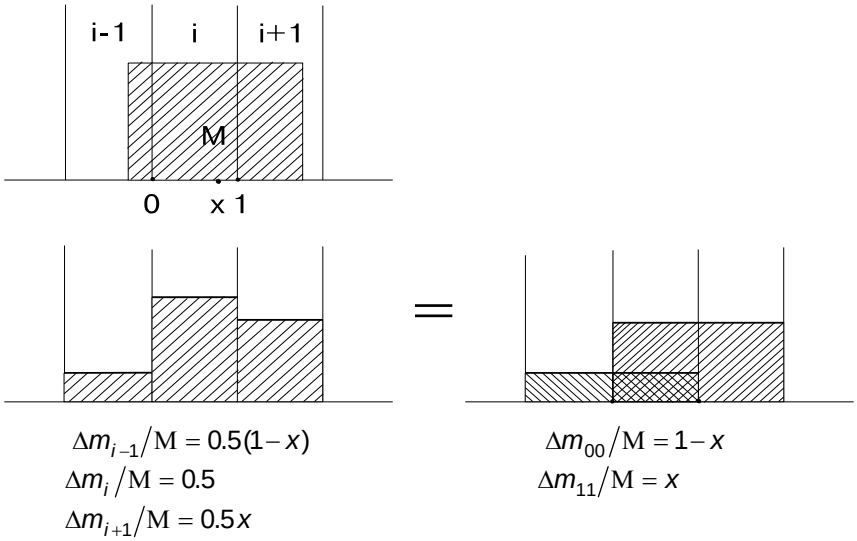

Sketch 2: *Projection of large particle M with co-ordinate x in i-cell (two-dimensional case is given by formulas (11))*

The combined distribution with grid is obtained by summing Δm_{kl} over all cells.

The projection of large particles on the grid is made as far as it is required. As a rule the model gives daily concentration fields.

The above described reconstruction makes it possible to introduce supplementary diffusion σ_0^2 added to σ_x^2 and σ_y^2, this will lead to uniform extension of similarity rectangle (Sketch 1). Numerical value σ_0^2 is defined by spatial and temporal steps of the model: $\sigma_0^2 = 2K_H\tau/\Delta x^2$, where K_H - horizontal diffusion coefficient. According to investigation [20], describing a number of model experiments made with various K_H and aimed at finding the best fit to measured concentrations of Cs^{137} from Chernobyl accident, optimum values are in the range of $3.3\cdot10^4 < K_H < 1\cdot10^5$ m^2/s. In the course of LPMOD verification using SO_2 air concentrations measured at the EMEP network calculations with various K_H were made in order to estimate suitable values. Our estimate is $K_H = 1.5\cdot10^4$ m^2/s. This value was used under modelling of Pb and Cd transport.

3.2 Horizontal transport in ASIMD

Finite - difference approximation is realized within the framework of classical "upwind scheme" for which numerical diffusion is well known. Compensation of numerical diffusion is made by correction of advection velocity depending on local gradients. The resulting velocity and real velocity are connected by non-linear equation.

Let us consider the one-dimensional equation (symbols are generally accepted):

$$\frac{\partial C}{\partial t} + u\frac{\partial C}{\partial x} = 0 \qquad (1)$$

and apply it to grid element $C_i^n = C(x_i, t_n)$, $x_i = (i + 1/2)\Delta x$, $t_n = n\tau$ (Δx - grid-size, τ-time step). The method used for devising difference approximations is complying with distribution:

$$\Delta C_i^k = P_i^k C_i^n, \quad k = i-1,\ i,\ i+1; \qquad (2)$$

where:

P_i^k = weights determining the contributions of element C_i^n to the neighbouring k-th cells.

In this presentation a standard scheme of directed differences for Eq.(1) is ($R_i = u_i\,\tau/\Delta x, u_i > 0$):

$$p_i^i = 1 - R_i, \qquad p_i^{i+1} = R_i. \tag{3}$$

Scheme (3) has artificial viscosity with coefficient:

$$\chi = \frac{1}{2}\left(u\Delta x - u^2\tau\right) \tag{4}$$

In order to compensate this viscosity we are to find an approximation for equation:

$$\frac{\partial C}{\partial t} + \frac{\partial}{\partial x}\left\{C\left(u + \frac{\chi}{C}\frac{\partial C}{\partial x}\right)\right\} = \chi\frac{\partial^2 C}{\partial x^2} \tag{5}$$

where:

$$\chi = \frac{1}{2}u\Delta x - \frac{1}{2}u^2\tau, \quad u = u + \frac{\chi}{C}\frac{\partial C}{\partial x} \tag{6}$$

In Eq.(6), χ and u are interrelated; exclusion χ from Eq.(6) results in a non-linear equation for u depending on u and local gradient:

$$u = u + \frac{1}{2}\left(u\Delta x - u^2\tau\right)\frac{1}{C}\frac{\partial C}{\partial x}. \tag{7}$$

Assuming for the i-th element:

$$\left(\frac{1}{C}\frac{\partial C}{\partial x}\right)_i = \frac{2}{\Delta x}\frac{C_{i+1} - C_i}{C_{i+1} + C_i} \quad \text{if } u_i > 0;$$
$$\left(\frac{1}{C}\frac{\partial C}{\partial x}\right)_i = \frac{2}{\Delta x}\frac{C_{i-1} - C_i}{C_{i-1} + C_i} \quad \text{if } u_i < 0; \tag{8}$$

and solving (7), we obtain:

$$R_i = \frac{-1 + \sqrt{1 + \left(a_i^2 - 1\right)R_i}}{a_i - 1} \quad \text{if } a_i \neq 1;$$
$$R_i = R_i \quad \text{if } a_i = 1; \tag{9}$$

Here, $R_i = u_i\tau/\Delta x$, $R_i = u_i\tau/\Delta x$, $a_i = C_{i\pm1}/C_i$ (signs +/- correspond to velocity one).

The second formula of Eq.(9) testifies on the lack of compensation of artificial viscosity in the region where $\partial C/\partial x = 0$, on smooth parts of the field or in maxima and minima. In such a way we obtain an analogue to "upwind" scheme ($u_i > 0$):

$$p_i^i = 1 - R_i, \qquad p_i^{i+1} = R_i. \tag{10}$$

where R_i is determined by formulae (9).

3.3 Vertical diffusion

As a rule splitting of 3-dimensional operator is made with separation of processes along z-co-ordinate:

$$\frac{\partial C}{\partial t} = \frac{\partial}{\partial z}K_z\frac{\partial C}{\partial z}, \quad \left(K_z\frac{\partial C}{\partial z}\right)_{z=z_0} = v_d C\left(z = z_0\right); \tag{1}$$

For solution (1) we use the variant of a simple scheme with conservation of 3 moments [17]. Here this scheme is developed for non-uniform grid.

At time step the simultaneous equations of conservation for mass, mass center co-ordinate and variance for the *i*-th grid element are solved ($m_i = C_i \Delta z_i$):

$$\begin{cases} m_i = \sum_{K=i-1}^{i+1} \Delta m_K, \\ m_i z_i = \sum_{K=i-1}^{i+1} \Delta m_K z_K, \\ m_i (K_{i-1/2} + K_{i+1/2})\,\tau = \sum_{K=i-1}^{i+1} \Delta m_K (z_K - z_i)^2; \end{cases} \tag{2}$$

Here Δm_K - input of m_i element to *i*-1, *i*, *i*+1 cells, τ - time step, $K_{i-1/2}, K_{i+1/2}$ - K_z values at the lower and upper boundaries of Δz_i cell.

The solution of set (2) with allowance that $z_{i-1} = z_i - 0.5(\Delta z_i + \Delta z_{i-1})$, $z_{i+1} = z_i + 0.5(\Delta z_i + \Delta z_{i+1})$ is represented by following algorithm:

$$\begin{aligned} \Delta m_{i-1} &= \frac{m_i}{P_- P_0}\left[6K_{i-1/2}\tau\right] \\ \Delta m_{i+1} &= \frac{m_i}{P_+ P_0}\left[6K_{i+1/2}\tau\right] \\ \Delta m_i &= m_i\left(1 - \frac{\Delta m_{i-1}}{m_i} - \frac{\Delta m_{i+1}}{m_i}\right) \end{aligned} \tag{3}$$

Here $P_- = \Delta z_i + \Delta z_{i-1}$; $P_0 = \Delta z_{i-1} + \Delta z_i + \Delta z_{i+1}$; $P_+ = \Delta z_i + \Delta z_{i+1}$.

For first cell *i*=1 we have:

$$\begin{aligned} &\Delta m_{i-1} = m_i v_d \tau \,/\, \Delta z_i;\ \Delta m_{i+1} = \frac{m_i}{P_+^2}\left[6K_{i+1/2}\tau\right]; \\ &\Delta m_i = m_i - \Delta m_{i+1} - \Delta m_{i-1}. \end{aligned} \tag{4}$$

For the last cell algorithm (3) is taken, it is assumed $\Delta z_{i+1} = \Delta z_i$.

The distribution of grid element m_i with weights $R_i^K = \frac{\Delta m_K}{m_i}$ should meet requirement:

$$\left(\frac{6K_{i-1/2}\tau}{P_- P_0} + \frac{6K_{i+1/2}\tau}{P_+ P_0}\right) \le 1. \tag{5}$$

which may be not fulfilled for two lower “thin” layers and we use integral weights:

$$\begin{aligned} R_i &= \frac{\Delta m_i}{m_i} = \exp\left\{-\frac{6\tau}{P_0}\left(K_+ + K_-\right)\right\} \\ R_{i-1} &= \frac{\Delta m_{i-1}}{m_i} = \left(1 - R_i\right)\frac{K_-}{K_+ + K_-} \\ R_{i+1} &= \frac{\Delta m_{i+1}}{m_i} = \left(1 - R_i\right)\frac{K_+}{K_+ + K_-} \end{aligned} \tag{6}$$

where: $K_+ = \frac{K_{i+1/2}}{P_+}$; $K_- = \frac{K_{i-1/2}}{P_-}$.

4 Parametrization of the Boundary Layer and Sinks

4.1 Boundary Layer

A system of parameters required for the description of local conditions of pollution dispersion consists of friction velocity u_*(m/sec), Monin-Obukhov length scale L(m), mixing layer height h (m), vertical diffusion coefficient profiles $K_z(z)$ (m^2/sec) which were devised on the bases of data on 1000 mb wind and temperature, roughness z_0. The roughness data were taken from the archive "Global Data Set for Land-Atmosphere Models" received in "International Satellite Land Surface Climatology Project" (ISLSCP). The database contains global data on roughness with resolution $1^0 \times 1^0$ averaged over a month. Monthly data for 1988 were included to the model. The interpolation on the EMEP grid was made by MSC-E specialists A.Gusev and S.Grigoryan.

The meteorological pre-processor is based on the method of energetic balance evaluation with further application of results of similarity theory, *van Ulden and Holtslag* [21, 22]. The parameter calculations were made for each 6-hour interval (0003, 0009, 0015, 0021 UTC).

The procedure is as follows:

1. The solar inclination angle φ is calculated for each point with geographical co-ordinates λ, ϕ (longitude, latitude) for a day of the year and time of the day.
2. According to φ a flux of solar short-wave radiation is calculated:

$$K^* = (990 \cdot \sin\varphi - 30) \cdot (1 - 0.75 N^{3.4})(1 - r), \quad (1)$$

where N - cloud coverage fraction; r - albedo, $r = 0.23$; $K^* = 0$, if $\varphi < 1.7^0$.

For 1990 we have no data on cloud coverage therefore it was assumed: $N = 1$ with precipitation events, $N = 0.4$ in all other cases.

3. Balance of solar short-wave radiation and long-wave radiation of the atmosphere and ground surface determines the positive flux of sensible heat in the atmospheric surface layer in the daytime:

$$H_0 = 0.4(K^* - 91 + 60 \cdot N) \geq 0. \quad (2)$$

At night ($H_0 < 0$) the heat flux cannot be presented in such a simple form. Here we take rougher estimate of heat flux than in [22], where the calculation gives of the dependence of temperature scale θ_* on u_* for night conditions. Taking into account that at velocities $u_* > 0.1$ m/s, θ_* is slightly dependent on u_* we took constant value $\theta_* = 0.065\ ^oK$ for negative fluxes.

4. Monin-Obukhov length scale is expressed as:

$$L = -\frac{\rho C_p T u_*^3}{kgH_0} = \frac{u_*^2 T}{kg\theta_*}, \quad (3)$$

where ρ is air density, C_p is the specific heat of dry air, k is von Karman`s constant, g is acceleration of gravity.

Friction velocity u_* determine universal wind profile in the surface layer:

$$u(z) = \frac{u_*}{k}\left[\ln(z/z_0) - \psi_m(z/L) + \psi_m(z_0/L)\right], \quad (4)$$

where:

$$\psi_m(z/L) = -17(1 - \exp(0.29\, z/L)), \quad \text{if} \quad L>0 \quad (5)$$

$$\psi_m(z/L) = (1 - 16\, z/L)^{1/4} - 1, \quad \text{if} \quad L<0 \quad (6)$$

(functions (5, 6) are presented in [22] as approximations valid for a wider range then $z<|L|$). Iteration method [23] applicable when wind and temperature data are available at two levels z became a standard method for the solution of two highly non-linear equations (3,4) with allowance for (5,6). We used less accurate technique. For this purpose supplementary empirical data of power dependence of wind on height were invoked:

$$u(z) = u_r \left(z / z_r \right)^p , \tag{7}$$

where $u_r = (u_{1000}^2 + v_{1000}^2)^{1/2}$, $z_r \cong 200\,\mathrm{m}$

According to data of *Irwin* [24] the following values for exponent p is assumed depending on stability:

$$p = \begin{cases} 0.10, & if \quad L > -200\,m \\ 0.16, & if \quad |L| > 200\,m \\ 0.32, & if \quad L < 200\,m \end{cases} \tag{8}$$

All calculations are made for z = 50 m. An appropriate exponent profile also defines wind speeds at lower 100 m layer. The wind rotation with height is neglected here.

Note the stability over the sea was assumed to be neutral and then [25]:

$$\begin{aligned} & u_* = \sqrt{C_d}\, u_{10}, \\ & C_d = 0.0012, \quad if \;\; u_{10} \le 11\,m/s, \\ & C_d = \left(0.49 + 0.065 u_{10} \right) \cdot 10^{-3}, \;\; if \;\; u_{10} > 11\,m/s, \end{aligned} \tag{9}$$

here C_d - friction coefficient, u_{10} - wind speed at 10 m.

5. The mixing layer height is a significant parameter for the evaluation of the coefficient of vertical diffusion $K_z(z)$. Using small K_z corresponding to the mixing layer top slowing down of the exchange between the layers is simulated. The temporal variation of the mixing layer height makes it possible to reproduce fumigation process.

   For the mixing layer height under stable and neutral conditions known expression is used:

$$h = C_1 u_* / f , \tag{10}$$

   where f - Coriolis parameter.

   (We rejected Zilitinkevitch formula for stable conditions because of unrealistic low of h, probably because this formular is asymptotic).

   For coefficient there is a great choice from 0.07 to 0.4. It was accepted: C_1 = 0.2.

   There are several methods for the determination of the convective mixing layer height based on solution of non-linear equation of type:

$$\frac{\partial h_C}{\partial t} = f\left(h_C, \overline{(w'\theta')}_s, \gamma, L, u_* \right) \tag{11}$$

   (γ - gradient of potential temperature above the mixing layer).

   For lack of some required data as well as inefficiency of application of numerical solution of this equation in each grid point, following direct dependence h_C from the surface heat flux was used:

$$h_C = 150 + 7H_0 \tag{12}$$

   where h_C in [m], H_0 in [W/m^2), derived while testing of the algorithm suggested by *Verver* [26].

6. Profiles of vertical diffusion coefficient in the surface layer follow from locally determined u_* and L mean for 6-hour interval [27]:

$$K_z(z) = \frac{k u_* z}{\phi(z/L)}, \tag{13}$$

where $\phi(z/L)$ - similarity function for heat:

$$\begin{aligned} \phi\,(z/L) &= 0.74\,(1-9z/L)^{-1/2}, \quad \text{if } L<0 \\ \phi\,(z/L) &= 0.74 + 4.7\,z/L, \qquad \text{if } L>0 \end{aligned} \tag{14}$$

Profile $K_z(z)$ were extended along the vertical of the boundary layer in the following way:

a) for the neutral layer the formula given by *Shir* [28] is used:

$$K_z(z) = k\,u_* z e^{-4z/h}\ , \tag{15}$$

b) for stable layer - *Rao and Snodgrass* profile [29]:

$$K_z(z) = \frac{k\,u_* z}{\phi(z/L)} e^{-0.9z/h}, \tag{16}$$

c) a profile similar to (15) was used for the convective layer:

$$K_z(z) = \frac{k\,u_* z}{\phi(z/L)} e^{-4z/h_C}, \tag{17}$$

which may lead to the underestimation of vertical diffusion under the conditions of convection.

In general there is a greater uncertainty of absolute values and distribution with the vertical $K_z(z)$ above the surface layer.

4.2 Parameters of dry and wet deposition for Pb and Cd

A flux of aerosol dry deposition carrying heavy metals is defined by expression:

$$F\left(x,y,z=z_0,t\right) = V_d\left(x,y,t\right)\cdot C\left(x,y,z_1,t\right) \tag{1}$$

where z_1 - the first calculation level along the vertical, z_1 = 50 m, V_d - variable over space and time the deposition velocity on the surface different for different metals.

According to *Sehmel`s* data [30] V_d variation range is three orders of magnitude.

When particles cross the laminar sublayer two maximum regimes of deposition is realised: 1 - for coarse particles - gravitational settling is decreasing with particles size decrease; 2 - for fine particles - deposition due to Brownian diffusion is decreasing with particle size increase. Thus for particles of intermediate size minimum deposition should be realized. It is observed for particles within the range 0.1-1.0 μm. These particles have rather small velocities, thousandth, hundredth fractions of 1 cm/s. Evidently these particles should dominate in the long-range transport.

According to *Milford and Davidson* data [1] spectrum maximum of aerosols with Pb and Cd is accounted for this size range. Median aerodynamic diameters for Pb and Cd equal to 0.55 μm and 0.84 μm respectively. When deposition process was parametrized we ignored the spectrum using MMD as “effective” particle size.

Besides particle sizes the deposition efficiency is influenced by meteorological conditions and surface properties and great difference between deposition velocities on land or sea are observed.

The parametrization of dry deposition velocity on a dry surface was made on the basis of *Sehmel`s* results [30], where similar calculations are given for V_d for a number of surfaces (z_0) and a set of turbulence states (u_*). For the assumption of “effective” sizes dependences $V_d\,(z_0)$ for individual u_*

were derived. In the double logarithmic scale they are represented by a family of parallel straight lines that allowed to accept the following approximations:

$$V_d^{land}(Pb) = \left(0.02\, u_*^2 + 0.01\right) \cdot \left(z_0 / 10^{-3}\right)^{0.33} \quad (2)$$

$$V_d^{land}(Cd) = \left(0.04\, u_*^2 + 0.02\right) \cdot \left(z_0 / 10^{-3}\right)^{0.30} \quad (3)$$

where: V_d^{land} [cm/s], u_* [m/s], z_0[m].

Results obtained with the model of *Lindfors et al* [25] which is a modified model of Williams [6] were used for the parametrization of deposition on the sea surface. The resistance analogy method is used, two layers are considered: turbulente and quasilaminar. In the quasilaminar layer fluxes are considered on both smooth and broken surface with sea spray that allows to consider the washout and coagulation with spray droplets. Using the results of this work we derived the following approximations for deposition velocities on the marine surface for Pb and Cd:

$$V_d^{sea}(Pb) = 0.15 \cdot u_*^2 + 0.013 \quad (4)$$

$$V_d^{sea}(Cd) = 0.15 \cdot u_*^2 + 0.023 \quad (5)$$

where: V_d^{sea} [cm/s], u_* [m/s].

Sink of pollutants due to precipitation scavenging is represented by a linear process:

$$\frac{\partial C}{\partial t} = -\Lambda C, \quad (6)$$

where washout coefficient Λ depends on many parameters of both pollutants and precipitation.

The models do not consider the complicated nature of the phenomena. The distribution of precipitations along the vertical is assumed to be uniform.

The flux of wet deposition from the layer of *h* depth is equal to:

$$F = C \Lambda h, \quad (7)$$

the same flux is represented as:

$$F = C_p I, \quad (8)$$

where C_p - concentration in precipitations, I - precipitation intensity.

Hence it follows that:

$$\Lambda = \frac{C_p}{C}\frac{I}{h} = \frac{W I}{h}, \quad (9)$$

where W - scavenging ratio equal to that of concentration in precipitation to concentration in the air. Orders of magnitudes of W for heavy metal particles are $\sim 10^5$ that testifies to the effective scavenging.

It set equal to 500000 for Pb and Cd. This value was also used in other long range transport models for Europe [12,13].

4.3 Spatial distributions of seasonally averaged meteoparameters

Meteoparameter distributions presented in fig.2-19 are a result of the parametrization of the boundary layer and dry deposition accepted in the models.

At first the used data of roughness length z_0 averaged over a month are given. For the comparison fig.2-3 demonstrate z_0 distributions for January and June. Essential differences are observed for these months - the major part of northern and eastern Europe is characterized by z_0 values exceeding 1 m. Both maps demonstrate elevated roughness of the coastal line.

Seasonally averaged meteoelements for two periods 00 and 12 UTC calculated for 1990 are presented in the following figures. Averaging over winter is made for January and February, for summer - June, July and August.

A great contrast for 00 and 12 is observed in the mixing layer heights in summer over land (fig.4-5). Characteristic values for the day-time are within the range of 1000-1500 m for the night-time - within the range 100-750 m (in regions with high roughness up to 1000 m). The latitudinal dependence of the mixing layer height is also observed. Over the sea h is practically uniform, $h < 500$ m. On the one hand it is connected with minor roughness, on the other - with the accepted in the model assumption on the neutral stratification of the boundary layer over the sea. Apparently data on the temperature of the sea surface would help to evaluate the atmosphere stability over the sea more accurately.

In winter such contrast between day and night is absent except southern regions (Sahara, Spain). Characteristic values h are observed in regions with high roughness 750-1000 m. Rather high values of h (compared with summer) are observed for the sea, to 1500 m. Higher values h for the winter period compared with data [31] is possibly connected with a high coefficient used in the diagnostic formula for h ($\sim 0.2 u_*/f$) for stable stratification. Note that peculiarities shown in the maps in the upper left and the lower right angles are probably conditioned by the objective analysis of wind. The spatial distribution of friction velocity u_* (fig.8-11) is correlated with z_0 distribution. The maximum value is observed in regions with high roughness reaching 1.5 m/s in winter. Over land in summer u_* is about 0.5 m/s.

The distribution of vertical diffusion coefficient $K_z(1)$ in the lower layer of the model grid is presented in fig.12-15. A big contrast is observed for periods 00 and 12 UTC for both summer and winter. For 12 UTC latitudinal dependence of $K_z(1)$ is pronounced. Mean value $K_z(1)$ is within the range of 25-100 m^2/s for 12 UTC period and 1-25 m^2/s for the period of 00 UTC. A similar pattern is observed for distribution $K_z(2)$ - vertical diffusion coefficient at the second model level (fig.16-19). Distributions of $K_z(1)$ and $K_z(2)$ are practically coincide for summer but $K_z(2)$ is higher than $K_z(1)$ for winter conditions because of non-uniform profile $K_z(2)$ in winter.

Dry deposition velocity distributions for lead (fig.20-23) demonstrate a dependence on the parameters defining turbulence intensity z_0 and u_*. Higher values are observed for 12 UTC compared with 00 UTC. Greater spatial non-uniformity is observed in winter. On the average winter velocities are higher than summer ones (see fig.52). The model predicts low velocities of dry deposition on the sea surface, $v_d < 0.05$ cm/s.

5 Results

5.1 Technical environment

The LPMOD and the ASIMD models consist of meteorological pre-processor and main simulation program which are written in FORTRAN and programmed to be run on the PENTIUM-100 computer.

In the final formulation the models have identical parametrization and differ only in the transport algorithms. The difference however is rather essential. The LPMOD-model operating half-steps requires greater computer resources (in addition to the more complex algorithm). The calculation with PENTIUM-100 of one component of the pollution for a year interval for grid 39×37×4 (actually 80×76×4 for LPMOD) takes about 6 hours while using LPMOD and about 20 minutes of ASIMD using.

5.2 Emission of Pb and Cd

The models require as input data annual emissions and the exact information of the location and the stack height of their sources. As emission inventories for Pb and Cd we used TNO maximum estimations for 1990 made under ESQUAD-project [32] recalculated for the EMEP grid with resolution 50×50 km^2 by MSC-E. The seasonal variations of lead and cadmium emissions are not significant [33] so they are not taken into account. The areal grid emission was diluted inside two lower model layers (0-100 m, 100-400 m), we allotted 0.8 of lead emission to the first model layer and 0.2 to the second model layer, for the cadmium emission that proportion was 0.5 : 0.5. Annual emissions amount to 48858 tonnes for lead and 1277 tonnes for cadmium in 1990.

The LPMOD model operates with “large particles” - emission portions given off by each 75 km grid cell. For “large particles “ distribution six cell moments are calculated during the transport simulation. Thus formally for LPMOD apart from emission distribution the all other moment distributions should be given. Naturally the second moments are equal to zero but the first two moments being source co-ordinates can be given if they are available. Initial emission distribution with 50 km resolution allows to determine large particle allocations to 75 km cells together with their co-ordinates. The ASIMD model has 150 km resolution so 50 km emission distribution is averaged for 150 km grid. The same emission distribution can be used in LPMOD, in that case “large particles” of sources have zero co-ordinates in accordance with adopted co-ordinate system.

5.3. Emission, deposition and concentration fields for Pb and Cd

Annual emission inventory for Pb in 1990 used in the model computations is shown in fig.24,25. Three data arrays should be used as emission input into the LPMOD model: proper emission as “large particles” mass and *x, y* - co-ordinates of the mass centres of large particles. The locations of particle centers and corresponding emission intensity only are shown in fig.25.

For Pb accumulated deposition and yearly averaged concentration in air and in precipitation simulated with both models are shown in fig.26-35 (For comparison the fields of the same type calculated by ASIMD and LPMOD are given side by side).

On the whole deposition and concentration fields calculated by both models are similar. The following differences may be noted. LPMOD presents higher levels of dry depositions in remote regions, for example in Greenland (Fig.26,27). At the same time dry deposition maximum predicted by ASIMD in Spain is not observed in dry deposition given by LPMOD. In the sites of high wet deposition LPMOD gives frequently higher levels of wet deposition (Fig.28,29), that is reflected by the total deposition computed as a sum of dry and wet depositions (Fig.30,31). For Pb concentrations in air predicted by ASIMD are slightly larger than ones predicted by LPMOD (Fig.32,33). The concentration in precipitation pattern is more irregular than wet deposition (Fig.34,35), LPMOD predicts the larger maxima than ASIMD. In particular the above mentioned maximum of dry deposition in Spain predicted by ASIMD corresponds to the maximum of wet deposition and concentration in precipitation predicted by LPMOD. Thus LPMOD overestimated slightly wet deposition in comparison with one of ASIMD.

For reference the concentrations in air computed by LPMOD with allowance for the source co-ordinates and without those are shown in Fig.36,37. The concentration distributions demonstrate large sensitivity of LPMOD to assignments of source allocations.

The following map package presents annual emission inventory (Fig.38,39), dry deposition (Fig.40,41), wet deposition (Fig.42,43), total deposition (Fig.44,45), concentration in air (Fig.46,47) and concentration in precipitation (Fig.48,49) for Cd computed by both models.

LPMOD sensitivity to Cd source allocations within grid cell is shown in Fig.50,51 as well. The same conclusion may be done in case of Cd: LPMOD underestimates slightly the concentration and overestimates wet deposition in comparison with ones predicted by ASIMD.

6 Assessment of results and discussion

6.1 Comparison of model results and observations

Model results for 1990 were compared with measurement data obtained at the PARCOM/ATMOS network. Tables 1,2 present comparison results.

Table 1: *Average concentrations in air (ng/m^3). Comparison of computed values versus measurements for 1990*

Site	Pb			Cd		
	measured	LPMOD	ASIMD	measured	LPMOD	ASIMD
B2b	104.0	46.9	62.0	-	-	-
DK1	17.0	15.8	17.7	0.3	0.42	0.45
D1	17.3	19.6	19.5	0.3	0.59	0.53
NL3	27.0	31.2	33.8	0.33	0.98	0.79
GB1	21.0	36.2	41.5	0.33	0.94	1.14
GB3	6.8	6.3	5.4	0.13	0.13	0.12
mean	32.2	26.0	30.0	0.278	0.612	0.606
corr.		0.88	0.82		0.88	0.85

Table 2: *Average concentrations in precipitation (μg/l). Comparison of computed values versus measurements for 1990*

Site	Pb			Cd		
	measured	LPMOD	ASIMD	measured	LPMOD	ASIMD
DK1	2.73	1.81	1.93	0.09	0.051	0.055
D1	-	-	-	0.15	0.066	0.055
F1	1.53	1.52	0.69	0.04	0.043	0.017
NL2	5.91	6.73	5.16	0.16	0.161	0.117
NL3	2.78	2.81	2.87	0.16	0.083	0.067
N2	0.20	0.69	0.75	0.06	0.019	0.020
N3	3.60	1.21	1.15	0.12	0.033	0.032
S2	2.05	1.77	1.67	0.08	0.057	0.054
GB1	4.93	5.60	5.18	0.40	0.171	0.133
GB2	11.17	10.3	13.77	0.35	0.300	0.378
GB3	3.03	2.92	2.21	0.13	0.073	0.054
GB4	0.88	0.68	0.33	-	-	-
mean	3.53	3.37	3.25	0.158	0.096	0.089
corr.		0.94	0.96		0.84	0.76

There is a high correlation between the modelled values and measurements. Results for Pb show the agreement between measured and modelled values. For Cd the models overestimate measured concentrations in air and underestimate concentrations in precipitation. That is probably due to the inadequate description of emissions for Cd of the models. In general while comparing the modelled values with measurements uncertainties of emissions and measurements should be taken into account. The overall uncertainty of the yearly averaged concentrations is estimated to be approximately 20 to 50% for the Western European countries where emission uncertainties are relatively small [33]. Thus the discrepancies between the measured and the modelled air concentrations of Cd exceed above mentioned interval.

Results of two models are close to each other. The small number of available observations makes it impossible to indicate preferable model.

There is information about measured mean long-term concentrations of Pb and Cd in Switzerland in 1985-1986 [3] and over the Mediterranean in 1991-1992 [34]. The aerosol concentration of remote sites data while compared with modelled values add the estimation of model performance. Air concentrations of Pb observed at 750-1550 m above sea level (Alpine region) are equal to 17.9-55.5 ng/m^3. Corresponding model values are 30-50 ng/m^3, Fig.32,33; EMEP gridcell (23,13). For Cd measured values are 0.3-0.69 ng/m^3, computed values are 0.5-1.0 ng/m^3.

At the land-based sampling stations in the Western Mediterranean (coast of France and Spain) following air concentrations are registrated, for Pb - 50-58 ng/m^3, for Cd - 0.36-0.60 ng/m^3. Model concentrations are 30-50 ng/m^3 for Pb and 0.5-1.0 ng/m^3 for Cd. Lower Pb and Cd concentrations were reported for Mediterranean Sea [35], mean values are equal to 10.5 ng/m^3 and 0.17 ng/m^3 correspondingly. That measurement data co-ordinate with modelled concentrations, Fig.32,33,46,47.

Besides the comparison of model results and observations of the estimations of particular model elements can be done. During the research of atmospheric input to the North Sea J.A. van Jaarsveld evaluated the mean dry deposition velocities of heavy metals for land and sea surface [11]. The similar monthly averaging of local dry deposition velocities used by our models was done. Results are shown in Fig.52. An unexpected agreement with van Jaarsveld`s values was found for both Pb and Cd. Mean values of dry deposition velocities for Pb and Cd calculated for other years (1989, 1991) show the rather slight influence of meteorological conditions. Seasonal variation of mean dry deposition velocities is observed that can be compared with the similar behaviour of dry deposition velocities of sulphate particles estimated for the Baltic region [25].

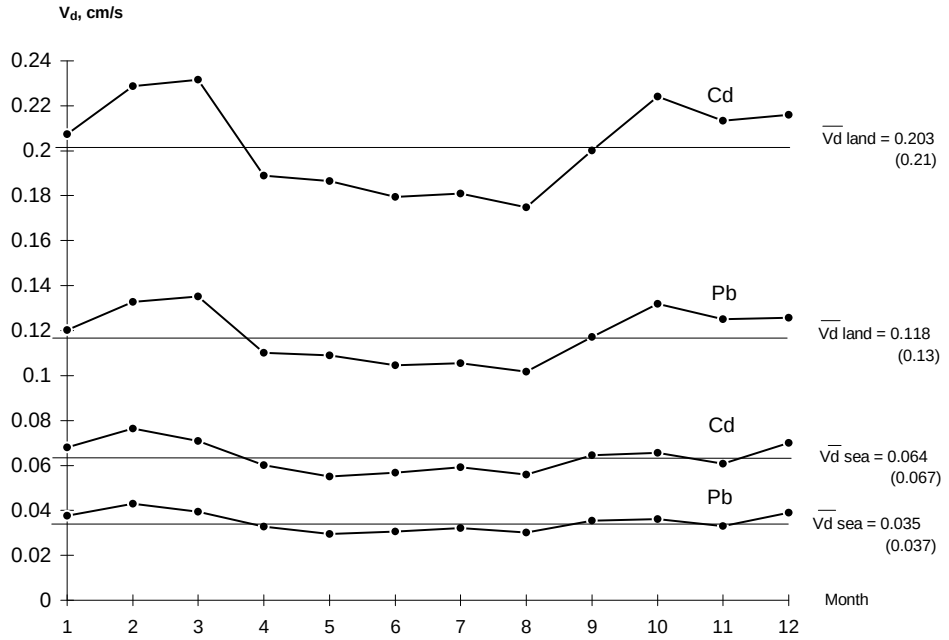

Fig.52 *Monthly averaged deposition velocities (cm/sec) for Pb and Cd separately for land and sea surface in 1990. Annual average dry deposition velocities are given as well. For comparison Jaarsveld`s data [11] are given in parentheses.*

6.2 LPMOD-ASIMD comparison

As is known a comparison of cumulative distributions is the most effective aid to the model evaluation. We can execute only the model-model comparison. The quantile-quantile plots of cumulative distributions of depositions or concentrations computed with LPMOD and ASIMD models are presented in Fig.53,54. For low percentiles LPMOD overestimates the values of depositions or concentrations in comparison with the values computed by ASIMD. Possible explanation is the different dispersive features of the models. In the remaining percentile interval the results of LPMOD and ASIMD agree much better. The curves for the concentration and dry deposition show overestimations of the highest values by ASIMD. That may be due to an overestimation of the scavenging rate by LPMOD.

The scatter diagrams of concentrations and depositions of Pb and Cd computed by ASIMD versus ones computed by LPMOD are compared in Fig.55,56. Statistical estimates (mean, correlation coefficient, slope, intercept) for all fields are presented in table 3.

Table 3: *Comparison of fields for Pb in 1990 computed by LPMOD versus computed by ASIMD*

Field	Average		Corr.	Slope	Intercept
	LPMOD	ASIMD			
dry dep. ($\mu g/m^2$)	358.61	407.15	0.965	0.802	32.19
wet dep. ($\mu g/m^2$)	979.08	946.28	0.969	0.927	101.75
tot dep. ($\mu g/m^2$)	1337.64	1353.46	0.967	0.872	149.87
conc. in air (0.1 ng/m^3)	122.92	146.90	0.948	0.729	15.74
conc. in prec. (0.01 $\mu g/l$)	175.11	174.12	0.975	0.910	16.59

The large correlation between corresponding fields computed by two models are observed. The main difference is in the relative intercept of the fields computed by LPMOD and ASIMD. That has been already remarked in the comparison of cumulative distributions. That disagreement of the models will be investigated during the following model evaluations.

On the whole results of both models are close and we can not prefer one to another now.

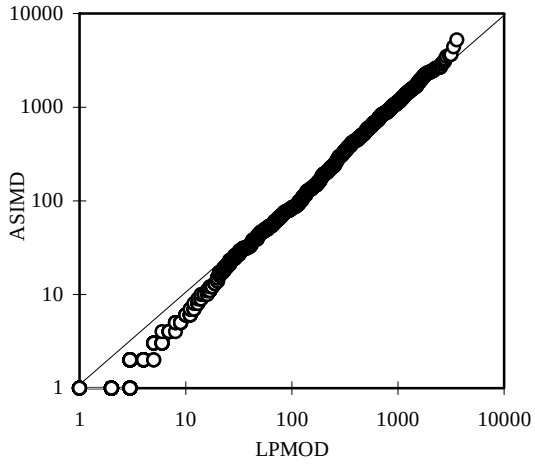

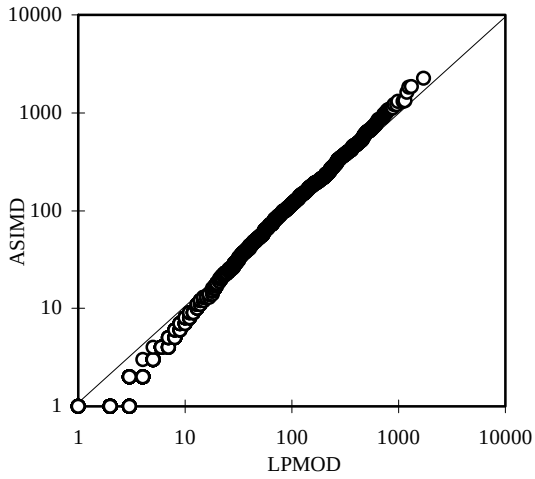

a. dry deposition in μg/m^2

d. concentration in air in 0.1 ng Pb/m^3

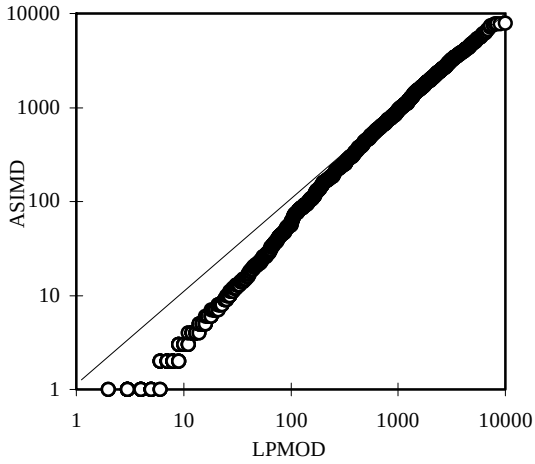

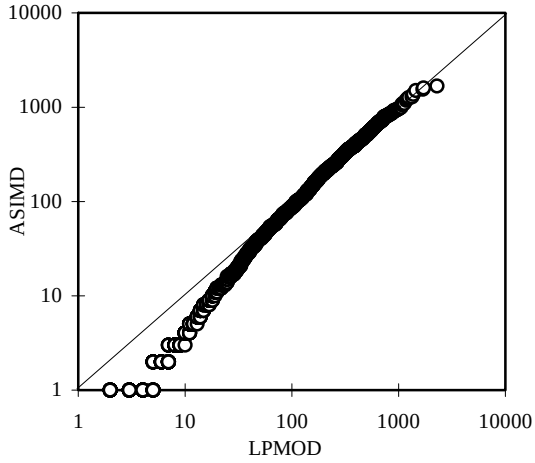

b. wet deposition in μg/m^2 e. concentration in precipitation in 0.01 μg/l

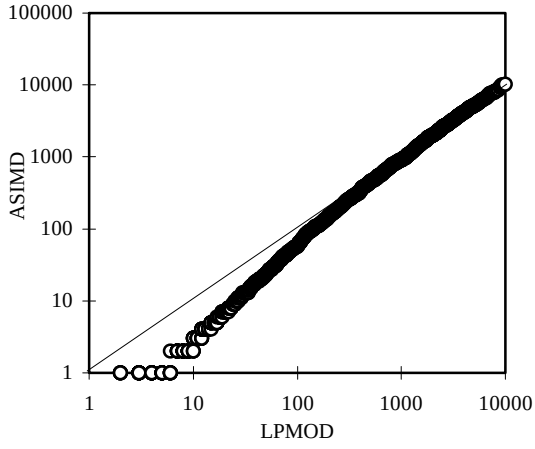

c. total deposition in μg/m^2

Fig.53 *Quantile-quantile plots of distributions of Pb estimated by LPMOD and ASIMD*

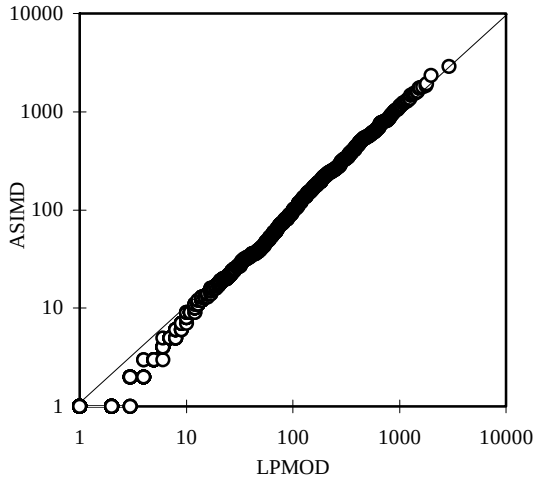

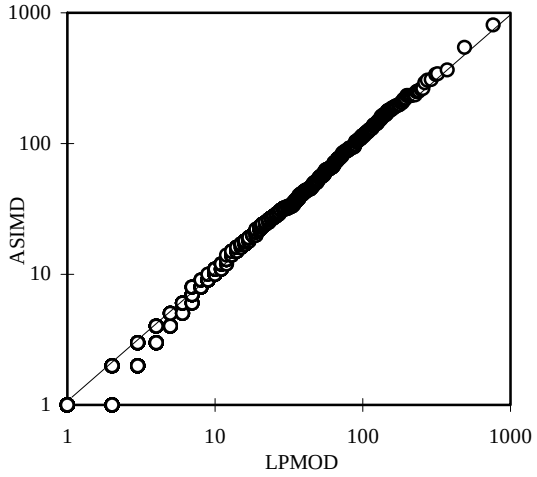

a. dry deposition in 0.1 μg/m^2

d. concentration in air in 0.01 ng/m^3

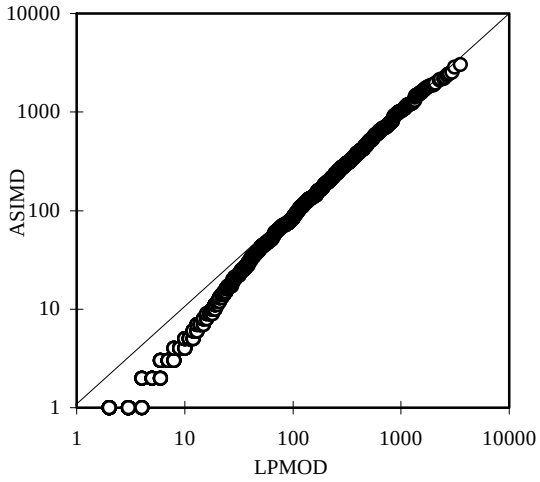

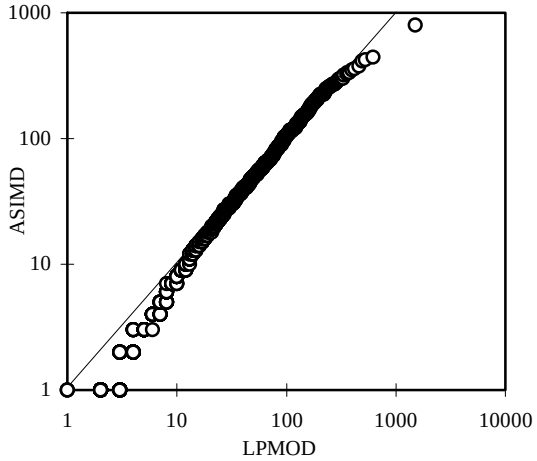

b. wet deposition in 0.1 μg/m^2 e. concentration in precipitation in 0.001 μg/l

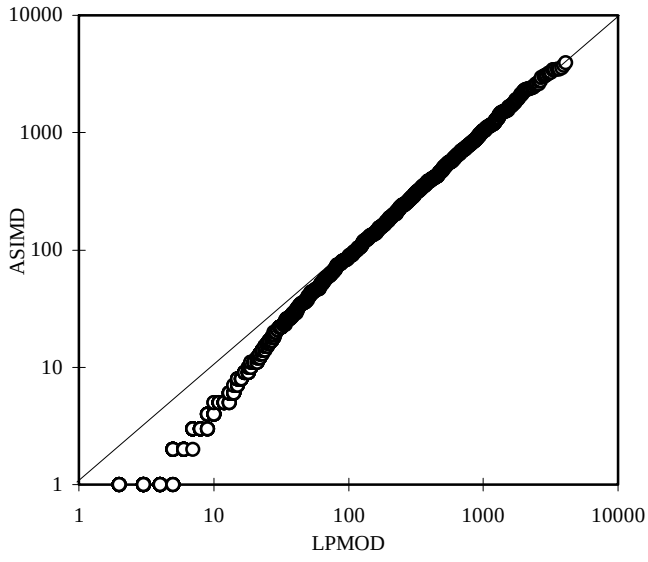

c. total deposition in 0.1 μg/m^2

Fig.54 *Quantile-quantile plots of distributions of Cd estimated by LPMOD and ASIMD*

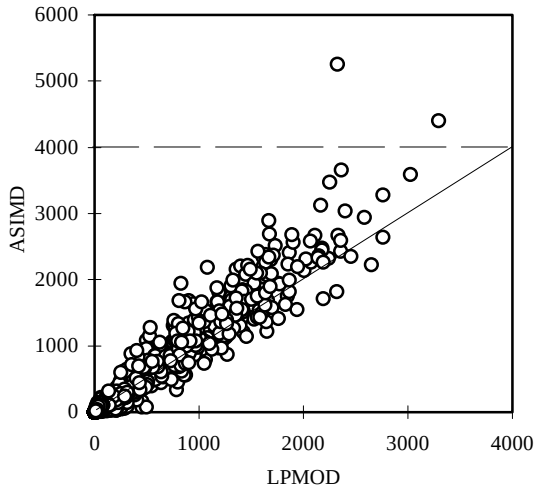

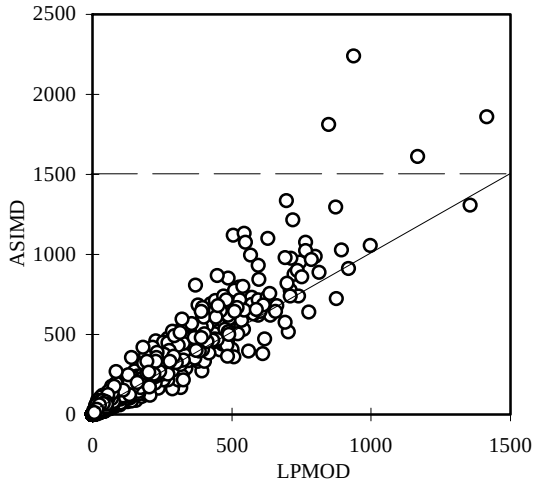

a. dry deposition in $\mu g/m^2$

d. concentration in air in 0.1 ng/m^3

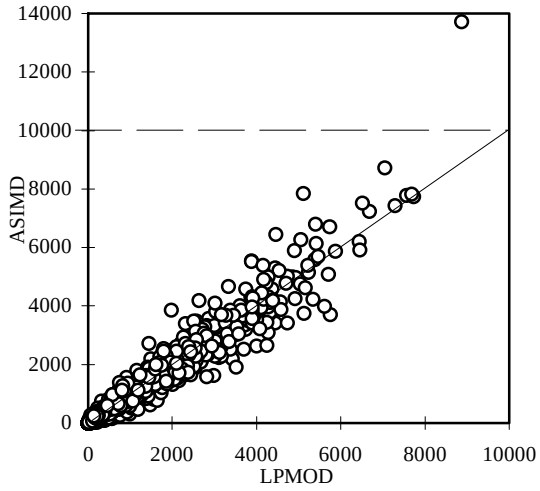

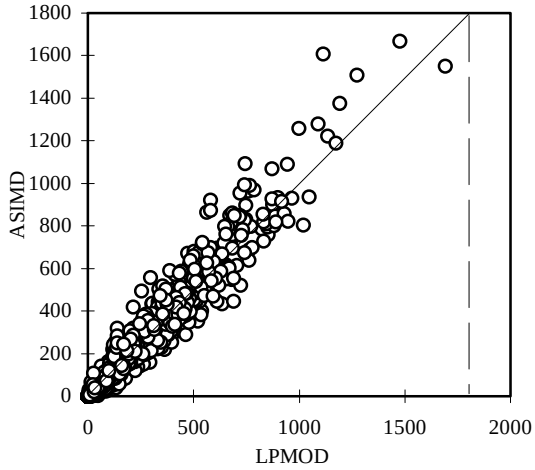

b. wet deposition in μg/m^2 e. concentration in precipitation in 0.01 μg/l

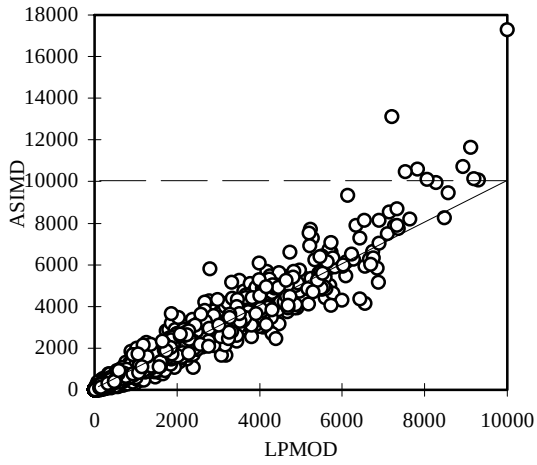

c. total deposition in μg/m^2

Fig.55 *Scatter plots of Pb distribution estimated by LPMOD and ASIMD*

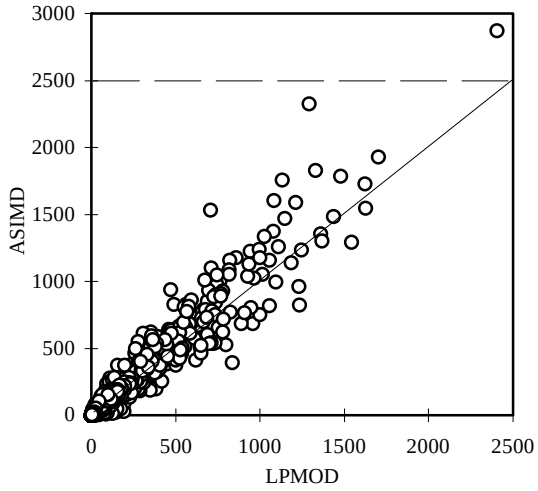

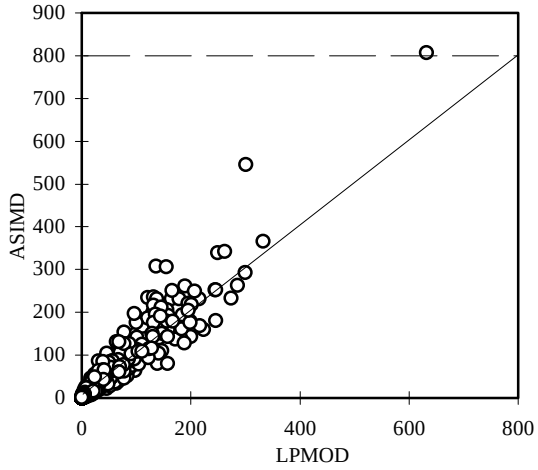

a. dry deposition in 0.1 μg/m^2

d. concentration in air in 0.01 ng/m^3

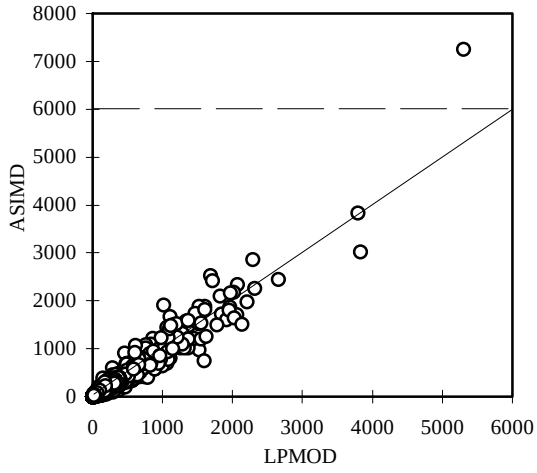

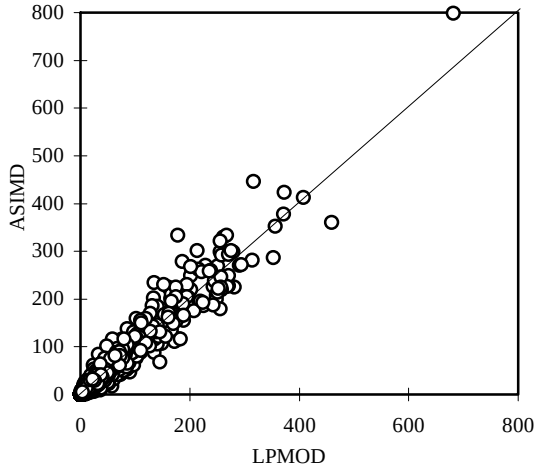

b. wet deposition in 0.1 μg/m^2 e. concentration in precipitation in 0.001 μg/l

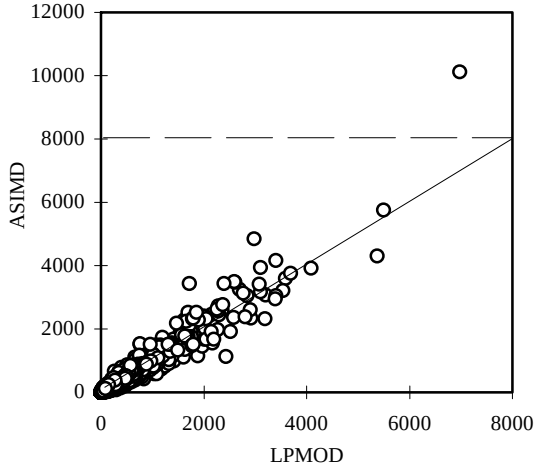

c. total deposition in 0.1 μg/m^2

Fig.56 *Scatter plots of Cd distributions estimated by LPMOD and ASIMD*

7 Conclusion and perspective

1. This report presents two versions of new regional 3d-model. The fine version (resolution 75 km) LPMOD uses the transport algorithm with conservation of six moments. The more rough version (resolution 150 km) ASIMD uses the asymmetric advection scheme with of advection velocity correction depending on local gradients. Meteorological pre-processor appreciates Boundary Layer stability, controlled parameters are heat flux, friction velocity, Monin-Obuchov scale and derived parameters (mixing layer height, vertical diffusivity, dry deposition velocity.) Gridded parameters are updated every six hours.

The maps of seasonally averaged meteoparameters for daytime and nighttime reflect expected dependencies on meteorological and geographical conditions. The estimations of mean dry deposition velocities for land and sea agree with known data. Those models are applicated for simulation of heavy metals long-range transport.

2. This report presents the simulation results of dispersion of Pb and Cd on the European scale in 1990. The main goals of the simulations are detail estimates of the depositions and comparative evaluation of two model versions.

The comparison of computed concentrations in air and in precipitation with measured ones at PARCOM stations shows an agreement of about 50% for Pb and of about 200% for Cd. The computed values are well correlated with the measured ones. The results of the both model versions are close to each other. The comparison of the modelled air concentrations with the concentrations measured in remote sites (Mediterranean, Alpine region) also shows reasonable agreement.

The comparison of the concentrations and depositions computed by LPMOD with ones computed by ASIMD demonstrates the similar means and good correlation but the appreciable intercept are noticed. The quantile-quantile comparison shows a good agreement in general but at the lower percentile interval LPMOD overestimates concentrations and deposition in comparison with ones computed by ASIMD. The certain overestimation of the wet deposition computed by LPMOD compared with one computed by ASIMD is observed.

For the rather limited validation of the models we can not answer formally the question “which model is better”. At the long-term integration the results of the ASIMD model are rather adequate to those of LPMOD. The ASIMD model can be used for massive and rapid calculations. However LPMOD having the better resolution and controlled dissipativity is to be applicated for the final computations. The short-term episodes can be also modelled with LPMOD. The following validation of the models of course is supposed. The several improvements of the models are planned. The submodel of initial plume growth and rise should be done.

3. The presented modelling results are the assessments based on the simple conceptions of aerosol behaviour with some heavy metals acting in the lower atmosphere. Many aspects of the behaviour of aerosols with heavy metals are uncertain because of complexity of physical process and the lack of measurements. It is known a little of the dependence of deposition velocities on the surface type, its roughness, atmosphere stability conditions. May be those uncertainties are even greater than those for gaseous compounds of sulphur and nitrogen. For the determination of wet deposition fluxes it is used a very rough approximation of effective scavenging without allowance for the complexity of the interaction of aerosol and precipitations (in a cloud and outside of it). Thus there is a great area of activity for further development of both operational and research modelling of heavy metals.

Data on emission should include the height of sources and the seasonal variations. Evaluation of particle spectrum composition could be allowed to distinguish the “heavy” part of the spectrum and to

separate local and regional processes. The same is true for the problem of the evaluation of the life-time of various components and for the problem of evaluation of the European background concentrations.

References

1. Milford J.B. and Davidson C.I. (1985) The sizes of particulate trace elements in the atmosphere - a review. Journal of the Air Pollution Control Association, vol.35, N 12, p.1249-1260.
2. Dulac F., Buat-Menard P., Ezat U., Melki S. and Bergametti G. (1989) Atmospheric input of trace metals to the western Mediterranean: uncertainties in modelling dry deposition from cascade impactor data. Tellus, 41B, p.362-368.
3. Gälli Purghart B.C., Nyffeler U.P. and Schindler P.W. (1990) Metals in airborne particulate matter in rural Switzerland. Atm.Env., 24A, p.2191-2206.
4. Müller J. (1986) Invariant properties of the atmospheric aerosol, J.Aerosol Sci., 17, N3, p.277-282.
5. Sehmel G.A. and Hodgson W.H. (1980) A model for predicting dry deposition of particles and gases to environmental surfaces. AICHE Symposium Series 76, p.218-230.
6. Williams R.M. (1982) A model for the dry deposition of particles to natural water surfaces. Atm.Env. 16, p.1933-1938.
7. Ruijgrok W., Davidson C.I. and Nicholson K.W. (1995) Dry deposition of particles. Tellus, 47B, p.587-601.
8. Slinn W.G.N. (1983) Predictions for particle deposition to vegetative surfaces. Atm. Env., 16, p.1785-1794.
9. Junge C.E. (1963) Air Chemistry and Radioactivity. Int.Geophys.Ser., vol.4, 382 pp., Academic, San Diego, Calif.
10. Tremblay A. (1987) Cumulus cloud transport, scavenging, and chemistry: Observations and simulations. Atm.Env., 21, 2345-2364.
11. van Jaarsveld J.A. (1992) Estimating atmospheric inputs of trace constituents to the North Sea: methods and results. Proc. 19th Technical Meeting of NATO-CCMS on Air Pollution and Its Applications, September 29-October 4, in Crete, Greece.
12. Alcamo J., Bartnicki J., Olendrzynski K. and Pacyna J. (1992) Results from a Climatological Model of Heavy Metal in Europe`s Atmosphere. Proc. 19th Technical Meeting of NATO-CCMS on Air Pollution and Its Applications, September 29-October 4, in Crete, Greece.
13. Bartnicki J., Modzelewski H., Szewczuk-Bartnicka H., Saltbones J., Berge E. and Bott A. (1993) An Eulerian model for atmospheric transport of heavy metals over Europe: model development and testing. DNMI. Tech.report N117. Norwegian Meteorological Institute, Oslo, Norway.
14. Galperin M., Sofiev M., Gusev A. and Afinogenova O. (1995) The approaches to modelling of heavy metals transboundary and long-range airborne transport and deposition in Europe, EMEP/MSC-E Tech.report 7/95, Moscow, Russia.
15. Pekar M. (1995) Algorithm of advection and diffusion with conservation of three moments of cell element. in Air Pollution III, ed. by H.Power, N.Moussiopoulos, C.A.Brebbia, vol.1, p.193-200, Computational Mechanics Publications.
16. Pekar M. (1995) Large particle model for the dispersion of primary pollution in various scales. EMEP/MSC-E, Technical report 2/95.
17. Pekar M.I. (1985) Conservative finite-difference schemes with minimization of the approximation viscosity for equation of air pollution transport and diffusion. MSC-E/EMEP, Technical Report 1/85.
18. Evaluation of long range atmospheric transport models using environmental radioactivity data from the Chernobyl accident. The ATMES Report, ed.by W.Klug, G.Graziani, G.Grippa, D.Pierce, C.Tassone, 1992, Elsevier Applied Science, p.229-234.
19. Smolarkiewicz P.K. (1983) A simple positive definite advection scheme with small implicit diffusion. Monthly weather review, v.III, p.479-486.
20. Ishikawa H. (1995) Evaluation of the effect of horizontal diffusion with Chernobyl data. J.Appl.Meteor., 34, p.1653-1665.
21. Holtslag A.A.M. and van Ulden A.P. (1983) A simple scheme for daytime estimates of the surface fluxes from routine weather data. J.Climate Appl.Meteor., 22, p.517-529.

22. van Ulden A.P. and Holtslag A.A.M. (1985) Estimation of atmospheric boundary layer parameters for diffusion applications. J.Climate Appl.Meteor., 24, p.1196-1207.
23. Berkowicz R. and Prahm L.P. (1982) Evaluation of the profile method for estimation of surface fluxes of momentum and heat. Atm.Env. 16, p.2809-2819.
24. Irwin J.S. (1979) A theoretical variation of the wind profile power-low exponent as a function of surface roughness and stability. Atm.Env., 13, p.191-194.
25. Lindfors V., Joffre S.M. and Damski J. (1991) Determination of the wet and dry deposition of sulphur and nitrogen compounds over the Baltic sea using actual meteorological data. Finnish Meteorological Institute Contributions N 4, Helsinki
26. Verver G.H.L. and Scheele M.P. (1988) Influence of non-uniform mixing height on dispersion simulations following the Chernobyl accident. Proc. 17th technical Meeting of NATO-CCMS on Air Pollution and Its Applications, Sept.19-22, 1988 in Cambridge, England
27. Businger J.A. (1973) Turbulent transfer in the atmospheric surface layer. In: Hangen D.A., editor. Workshop on Micrometeorology. AMS, Boston MA, p.67-100.
28. Shir C.C. (1973) A preliminary numerical study of atmospheric turbulent flows in the idealized boundary layer. J.Atmos. Sci., 30, p.1327-1339.
29. Rao K.S. and Snodgrass H.F. (1979) Some parametrization of the nocturnal boundary layer. Boundary Layer Meteorology, 17, p. 15-28.
30. Sehmel G.A. (1980) Particle and gas deposition: a review. Atm.Env. 14, p.983-1011.
31. Jakobsen H.A., Berge E., Iversen T. and Skalin R. (1995) Status of the development of the multilayer. Eulerian model. EMEP/MSC-W, Note 3/95, Norwegian Meteorological Institute, Oslo, Norway.
32. Berdowski J.J.M., Pacyna J.M. and Veldt C. (1994) Emission. In: The impact of atmospheric deposition of non-acidifying pollutants on the quality of European forest soils and the North Sea. Main report of the ESQUAD project (ed. K.D. van den Hout) IMW-TNO report 93-329, Delft, The Netherlands.
33. Baart A.C., Berdowski J.J.M. and J.A. van Jaarsveld (1995) Calculation of atmospheric deposition of contaminants on the North Sea (ed. J.H.Duyzer). TNO-MEP-R95/138, Delft, The Netherlands.
34. Kubilay N. and Saydam A.C. (1995) Trace elements in atmospheric particulates over the Eastern Mediterranean: concentrations, sources, and temporal variability. Atm.Env.29, p.2289-2300.
35. Chester R., Nimmo M., Alarcon M., Saydam C., Murphy K.J.T., Sanders G.S. and Corcoran P. (1993) Definiting the chemical character of aerosols from the atmosphere of the Mediterranean sea and surrounding regions. Ocean. Acta 16, p.231-246.